Journal of Alloys and Compounds 501 (2010) 136–142

Contents lists available at ScienceDirect

Journal of Alloys and Compounds

journal homepage: www.elsevier.com/locate/jallcom

Ab-initio determination of X-ray structure factors and the Compton profiles of CdO

M.S. Dhaka[a], U. Paliwal[b], G. Sharma[c], M.C. Mishra[d], K.B. Joshi[b,*], R.K. Kothari[d], B.K. Sharma[d]

[a] Department of Physics, Engineering College Bikaner, Bikaner 334004, India
[b] Department of Physics, M.L. Sukhadia University, Udaipur 313002, India
[c] Department of Physics, Banasthali University, Banasthali 304022, India
[d] Department of Physics, University of Rajasthan, Jaipur 302004, India

ARTICLE INFO

Article history:
Received 21 January 2010
Received in revised form 3 April 2010
Accepted 7 April 2010
Available online 20 April 2010

PACS:
71.15.Ap
71.15.Dx
71.15.Mb
71.15.Nc
71.20.Nr
78.70.−g

Keywords:
Band structure
Cadmium oxide
Compton profile
Equation of state
LCAO method
X-ray structure factors

ABSTRACT

X-ray structure factors and Compton profiles of CdO are presented in this work. The theoretical calculations are performed employing the first-principles linear combination of atomic orbitals (LCAO) method using the CRYSTAL code. The computations are made considering the Perdew–Burke–Ernzerhof (PBE) correlation energy functional and Becke's ansatz for the exchange. The computed X-ray structure factors for B1 structure are compared with the available experimental data. To compare the averaged theoretical Compton profile, first ever measurement on polycrystalline CdO is reported using 5Ci ^{241}Am Compton spectrometer. The ionic model calculations have been used to estimate charge transfer in CdO. The agreement is, however, better with the LCAO calculation. The first-principles calculations of equilibrium lattice constants, bulk moduli and its pressure derivative of competing B1 and B2 phases of CdO are also reported and compared with the available results. The computed transition pressure for B1 → B2 structural phase transition is in good agreement with the experimental findings. Moreover, the electronic band structures show that B1 phase has indirect band gap of 0.43 eV in reasonable agreement with the experiments and B2 phase exhibits negative band gap of 0.9 eV.

1. Introduction

Most of the IIB–VIA oxides have a wide range of applications. For instance, these are used as transparent conducting oxides in photovoltaic devices, liquid-crystal displays, and light-emitting diodes [1–3]. The semiconducting compounds of this family crystallize mostly in the zincblende (B3), wurtzite (B4) or both structures. The binary oxides of Mg, Zn, Cd, and related alloys have the band gap around 0.5–7.7 eV [4–6]. It has been reported that electrical and optical properties of CdO get considerably modified due to metallic doping [7–11]. Consequently, these have emerged as credible alternatives for lighting applications in a wide range of wavelength. Cadmium oxide (CdO), one of the important binary oxides, exhibits interesting structural, electronic and optical properties. It has been studied in various forms such as rocksalt (B1), CsCl-type (B2), zincblende (B3) and wurtzite (B4) structures. Unlike other II–VI semiconductors B1 is the stable phase of CdO under ambient conditions. A number of calculations have shown that B2 is energetically competing structure of CdO. It has attracted a few structural studies with a view to foresee possibilities of structural transitions or to see the nature and magnitude of band gaps in alternative structures. Recently, Peng et al. [12] have studied the pressure dependent Poisson ratio, Debye temperature and shear elastic wave velocities using plane wave pseudopotential method. Zhu et al. [4] applied the full potential-linearised augmented plane wave (FP-LAPW) method to study phase stability, bands alignment in II–VI oxides including CdO. Ground state and metastable states of CdO are analysed and band offsets for the B3 structure are reported by Duan et al. [13]. A pressure induced phase transition from B1 to B2 type is predicted at 89 GPa by Moreno and Takeuchi [14] on the basis of FP-LAPW method which was experimentally observed by Liu et al. at 90.6 GPa [15]. The electronic density of states and band structure for CdO were reported using LCAO method by Dou et al. [16] and compared with the X-ray photoemission spectroscopy (XPS) measurements.

* Corresponding author. Tel.: +91 294 2423641; fax: +91 294 2423639.
E-mail address: k_joshi@yahoo.com (K.B. Joshi).

0925-8388/$ – see front matter © 2010 Elsevier B.V. All rights reserved.
doi:10.1016/j.jallcom.2010.04.060

King et al. [17] reported valence band density of states for the B1 phase applying high-resolution XPS and observed effect of shallow semicore *d* levels on valence bands in CdO. The experimental X-ray structure factors are reported by Rantavuori and Tanninen [18] which were compared with the simple theoretical model. It is established that the Compton scattering is an important technique to study the electronic properties of solids [19–21]. In this technique, essentially, one determines the one-dimensional projection of the ground state 3D momentum density $\rho(\mathbf{p})$ along p_z. Since, it can be measured through the Doppler shift of Compton scattered photons by electrons in motion [19–21], the Compton profile study offers a stringent test on the quality of theoretical framework employed to generate $\rho(\mathbf{p})$ for solids. To our knowledge, no such study on CdO is reported so far.

Our aim in this work is to apply first-principles LCAO method to compute X-ray structure factors, Compton profile and anisotropy in directional Compton profiles of CdO. The computed X-ray structure factors are compared with the experimental data of Rantavuori and Tanninen [18]. To compare the calculated Compton profile, the first ever measurement has been performed on polycrystalline CdO using 5Ci ^{241}Am Compton spectrometer. The anisotropy measurements could not be performed due to non-availability of single crystals. We have also performed the first-principles total energy calculations for the competing B1 and B2 structures to compute equilibrium lattice constant, bulk modulus, pressure derivative of bulk modulus and the structural phase transition pressure. These quantities are compared with the available experimental and theoretical results. Moreover, the electronic band structures calculations for the B1 and B2 structures are also performed to report band gaps.

All properties in the equilibrium state are computed following the first-principles LCAO method based on the density functional theory (DFT) embodied in the CRYSTAL code. To estimate charge transfer through Compton profile data, simple ionic model based on free atom profiles has been employed. Unless stated, all quantities are in atomic units (a.u.) where $e = \hbar = m = 1$ and $c = 137.036$, giving unit momentum = 1.9929×10^{-24} kg m s^{-1}, unit energy = 27.212 eV and unit length = 5.2918×10^{-11} m.

2. Theory and computational details

2.1. The DFT-LCAO theory

The *ab-initio* periodic LCAO calculations are performed wherein one solves the Kohn-Sham equations self-consistently under the DFT [22,23]. A few fundamental schemes exist to construct Hamiltonian for the periodic solids. Hartree–Fock (HF) approximation and the DFT [22] are the well known approaches among these schemes. In HF, according to Kohn and Sham [24], when exchange and correlation appear as a non-local effective potential, the exchange potential is included exactly and additional terms describe the correlation effects approximately [24]. In the DFT, both exchange and correlation effects are included but approximately in practice. The effectiveness largely depends on the systems under investigation. There are a number of functionals existing in literature to treat exchange and correlation under the DFT. Naturally, on account of having different Hamiltonians, the schemes project different band structure and total energy with small differences due to various correlation and exchange potentials. The CRYSTAL code [25] provides a platform to calculate electronic structure of periodic systems with Gaussian basis employing HF, DFT and the hybrid schemes. In this method, each crystalline orbital $\psi_i(\mathbf{r},\mathbf{k})$ is a linear combination of Bloch functions $\varphi_\mu(\mathbf{r},\mathbf{k})$ defined in terms of local functions $\varphi_\mu(\mathbf{r})$, normally referred as atomic orbitals. The local functions are expressed as linear combination of certain number of individually normalized Gaussian type functions. For Cd and O, the local functions were constructed from the Gaussian type basis sets [26].

The Kohn–Sham Hamiltonian was constructed following the prescription of Saunders et al. [25]. The calculations were performed for competing rocksalt (B1) (space group $Fm\bar{3}m$) and CsCl-type (B2) (space group $Pm\bar{3}m$) structures of CdO. As PBE [27,28] is one of the reasonably successful correlation functional employed to study properties of 4d binary compounds [29], we have used this in our calculations to treat correlation together with the Becke's ansatz for the exchange potential. The self-consistent calculations were performed considering $455\vec{k}$ points in the irreducible Brillouin zone with sufficient tolerances. To achieve self-consistency mixing of successive cycles was considered and the self-consistency was achieved within 21 cycles.

The equations of states for the B1 and B2 structures with different correlation functionals were generated following the prescription of Birch [30]. The deduced $E(V)$ curves were used to derive structural properties.

The static structure factors are very useful in analyzing the X-ray diffraction data, charge density, and thereby charge transfer and bonding in solids [31]. One can obtain the structure factor $S(\mathbf{k})$, for a given reflection line identified by $(h\,k\,l)$ from the following expression:

$$S(\mathbf{k}) = \int_V \rho(\mathbf{r})\exp(-i\mathbf{k}\cdot\mathbf{r})d\mathbf{r}, \tag{1}$$

where the integration is performed over the unit cell giving total number of electrons in the unit cell for $\mathbf{k} = 0$.

Compton profile is derived from the ground state momentum density distribution in solids. In the independent particle model the momentum density $\rho(\mathbf{p})$ is given by [19–21]:

$$\rho(\mathbf{p}) = (2\pi)^{-3}\sum\left|\int \psi(\mathbf{r})\exp(i\mathbf{p}\cdot\mathbf{r})\right|^2, \tag{2}$$

where $\rho(\mathbf{p})$ is the three-dimensional momentum distribution and $\psi(\mathbf{r})$ represents the electron wave function. The summation is over all occupied states. The Compton profile can be derived from the ground state momentum density $\rho(\mathbf{p})$ as:

$$J(p_z) = \int_{-\infty}^{+\infty}\int_{-\infty}^{+\infty}\rho(\mathbf{p})dp_x dp_y. \tag{3}$$

It is interesting to note that $S(\mathbf{k})$ is deduced from the ground state charge density distribution whereas Compton profile is deduced from the ground state momentum density distribution. Together these two quantities allow to study properties of materials in real and momentum space. In the present case, the valence Compton profiles were calculated over the range of 0–9 a.u. to count 8.718 electrons in the compound.

2.2. Ionic model

The theoretical Compton profiles of CdO for various ionic arrangements were calculated from the free atom profiles of Cd and O taken from Biggs et al. [32]. The valence profiles for various $Cd^{+x}O^{-x}$ ($0.0 \le x \le 2.0$ in step of 0.1) configurations were calculated by transferring x number of electrons from 5s shell of Cd to the 2p shell of O and the valence profiles for $Cd^{+x}O^{-x}$ were added to core contributions to get the total profiles. All profiles were then appropriately normalized to compare with the experimental data.

3. Compton profile measurement and data analysis

The ^{241}Am gamma-ray Compton spectrometer, earlier described by Sharma et al. [33], has been employed for measurement in this

work. The sample was powder of 99.99% purity. It was kept at room temperature (22 °C) in a circular cell with mylar windows on both the front as well as the back sides. The thickness of the CdO powder sample was 3.2 mm with effective density 2.29 g/cm^3. The sample cell was kept vertical by affixing it on the back of a lead covered brass slab having a hole of 18 mm diameter. The chamber was evacuated to about $\sim 10^{-2}$ Torr to reduce contribution of air scattering. The incident gamma-rays of 59.54 keV energy were scattered by the sample through a mean angle $165 \pm 3.0°$. The scattered radiations were detected and analysed using a HPGe detector (Canberra model GL0110P) and associated electronics like spectroscopy amplifier (Canberra, 2020 model), an analog to digital converter (Canberra, 8701 model) and a multichannel analyzer (Canberra, S-100). To reduce pile-up contribution in the profile, the experiment was performed with 1 μs shaping time. As a confirmation of this, we measured the Compton profile of Cd metal. Our values were in close agreement with published data [34]. The spectrum was collected in a multichannel analyzer (MCA) with 4096 channels having a channel width of 20 eV, which corresponds to about 0.03 a.u. of momentum on electron momentum scale. The spectrometer had an overall momentum resolution of 0.6 a.u. (Gaussian FWHM), which includes the detector resolution and the geometrical broadening of the incident and the scattered radiations. The Compton scattering spectra were measured for 44 h to accumulate 2.6×10^6 integrated counts in the Compton profile region. The drift in the electronic system was checked using a weak ^{241}Am calibration source. To correct for the background, which is mainly due to scattering from sample holder, mylar and cosmic background, measurement was made with the sample holder only. Thereafter, the measured background was subtracted from the raw data point by point after scaling it to the actual counting time. The measured profile was then corrected for the effect of detector response function, energy dependent absorption and scattering cross-section according to the scheme described by Williams [19] and Warwick group [35]. The data reduction for the detector response function was restricted to striping-off the low energy tail of the resolution function and after converting the Compton profile into momentum scale, Monte Carlo simulation of the multiple scattering was performed [36]. The contribution of the multiple scattering was found to be 4% in the momentum region −10 to +10 a.u. Thereafter, the profile was normalized to free atom Compton profile [32] for the area of 22.859 electrons in the momentum range from 0 to +7 a.u. The contribution of 1 s electrons was excluded as they do not contribute in the scattering.

4. Results and discussion

4.1. Equilibrium phases

As stated earlier, we studied two polymorphs of CdO: the B1 rocksalt structure with space group $Fm\bar{3}m$ and the B2 CsCl-type structure with $Pm\bar{3}m$ space group. These phases are the six-fold coordinated NaCl or eightfold-coordinated CsCl structures. To determine the equilibrium lattice parameters for the two structures, the total energy was calculated. Using the Birch equation of state (EOS) [30], we obtained the energy–volume dependences $E = E(V)$. The corresponding fits are given in Fig. 1. Both structures are studied adopting Becke's ansatz for exchange and PBE correlation functional. In Table 1 the deduced equilibrium lattice constant a, isothermal bulk modulus B_0, and its pressure derivative $B' = -(dB/dp)_{p=0}$ are presented. For comparison, our results, recent measurements and other *ab-initio* calculations are also presented here. It can be seen that calculated lattice constants are $a = 4.779$ and 2.96 Å for B1 and B2 structures, respectively. The corresponding experimental lattice constants are 4.704 and 2.86 Å which indicates

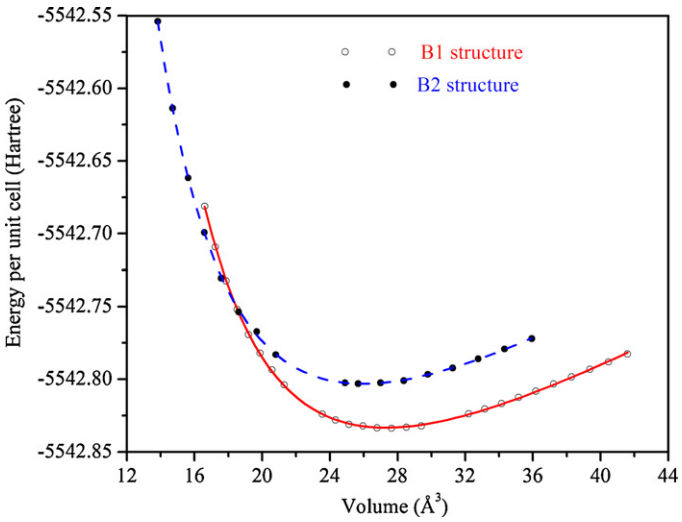

Fig. 1. First-principles energy–volume curves for B1 and B2 structures of CdO calculated using DFT-LCAO method. The scattered points show calculated energies and the solid and dashed lines show the fitted $E(V)$ curves according to Birch equation of state.

that theory overestimates a by 1.6% (for B1) and 3.5% (for B2). Considering the fact that generalised gradient approximation (GGA) generally overestimates the lattice parameters [29], our results can be taken to be in good agreement. It is to be noted that the pseudopotential under local density approximation (PP-LDA) unusually overestimates the lattice constants [12]. The pressure coefficients computed by DFT-LCAO are close to the experimental data. While comparing computed bulk modulus, one observes that all calculations underestimate the bulk moduli of the two structures. The bulk moduli of B1 and B2 structures are 18% and 29% smaller than the experimental data. These deviations are well within the limit of 30% [29] suggesting a reasonably good agreement.

Now we discuss the structural transition B1 → B2 in CdO. The transition pressure is obtained from the enthalpy calculations. The calculated enthalpies of the two phases are plotted in Fig. 2. The figure reveals structural transition pressure (P_t) at 102.5 GPa. The transition is experimentally reported at 90.6 GPa. As noted earlier [37,38], a hysteresis exists between forward and backward transition and generally the middle value is conventionally taken as an approximation to find equilibrium transition pressure in experiments. In view of this, the predicted transition pressure is in good agreement with the experiment. The comparison of computed structural parameters with the experimental data ensures reliability of our calculations.

Table 1
Calculated structural properties of CdO in the B1 and B2 structures.

		PP[a] LDA	PP[b] GGA	FP-LAPW[c] GGA	DFT-LCAO PBE-GGA	Expt.[d]
B1	a_0 (Å)	4.780	4.779	4.770	4.779	4.704
	B_0 (GPa)	125.340	130.500	121.030	119.850	147.000 ± 4.0
	B'	4.910	5.000	4.190	4.290	4.200 ± 0.1
B2	a_0 (Å)	2.948	–	2.960	2.960	2.860
	B_0 (GPa)	128.120	–	116.450	118.980	169.000 ± 7.0
	B'	4.920	–	4.070	4.010	4.660
P_t (GPa)		83.10	85.00	89–91	102.500	90.600 91–102

[a] Ref. [12].
[b] Ref. [39].
[c] Ref. [14].
[d] Ref. [42].

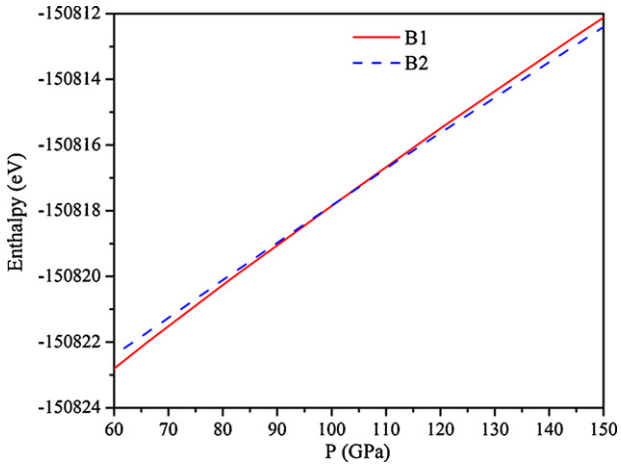

Fig. 2. Enthalpy calculated from first-principles for B1 and B2 structures of CdO using PBE correlation functional. At the transition pressure (P_t) 102.5 GPa curves cross each other.

4.2. X-ray structure factors

In Table 2, we give the computed X-ray structure factors for a few reflection lines of B1 and B2 structures of CdO. The correction due to the Debye Waller (DW) factor is considered for B1 structure only. For this, each computed structure factor is multiplied by $\exp(-0.71(\sin\theta/\lambda)^2)$ taking the proposed factors $b_{Cd} = 0.54$ and $b_O = 0.17$ for Cd and O, respectively [18]. The only experimentally available structure factors of CdO are also listed in the table for comparison. From the table, it is obvious that up to (2 2 0) reflection the agreement is good and within experimental errors. Beyond this, differences are larger than the experimental errors. For the higher reflection lines, the deviation from measurement is larger which may be due to the DW factor. The factor is larger (~91%) as the measurement was performed at 80 K. Also some disagreement may probably be due to omission of the anomalous dispersion correction in the experimental data. There is enough scope for experiments with high statistical accuracy at synchrotron radiation facilities which would provide more accurate DW factors enabling rigorous comparison. The structure factors for B2 may be beneficial for the structural refinement using X-ray and or neutron diffraction techniques.

4.3. Electronic band structures

The electronic band structures for the B1 and B2 phases of CdO are plotted in Figs. 3 and 4, respectively. It is obvious from Fig. 3

Table 2
Computed X-ray structure factors of CdO crystallising in the B1 and B2 structures. For B1, the structure factors are multiplied by the Debye Waller factor. For B2, the calculated values are directly given.

B1			B2	
[h k l]	DFT-LCAO	Expt.[a]	[h k l]	DFT-LCAO
1 1 1	32.77	33.64 ± 0.34	1 1 0	41.68
2 0 0	42.38	43.25 ± 0.86	2 0 0	34.83
2 2 0	34.92	36.60 ± 1.10	2 1 1	30.64
3 1 1	24.75	27.08 ± 0.27	2 2 0	27.80
2 2 2	29.98	33.10 ± 0.33	3 1 0	25.74
4 0 0	26.37	28.96 ± 1.16	2 2 2	24.22
3 3 1	19.91	23.25 ± 0.23	3 2 1	23.02
4 2 0	23.62	27.20 ± 0.54	4 0 0	22.03
4 2 2	21.42	25.51 ± 0.78	4 1 1, 3 3 0	21.22
5 1 1, 3 3 3	16.70	20.77 ± 1.04	4 2 0	20.53

[a] Ref. [18].

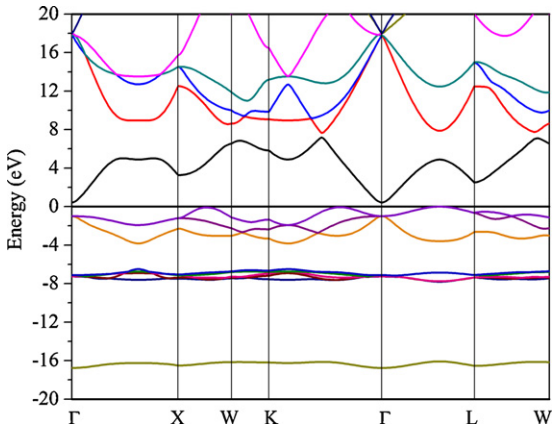

Fig. 3. Energy band structure for B1 phase of CdO obtained from the PBE correlation and Becke's exchange functional. The indirect band gap is 0.44 eV along the Σ (i.e. Γ–K) direction.

that CdO in B1 phase is a semiconductor with indirect band gap 0.43 eV. Other correlation functionals, not described here, give band gap within 0.43–0.5 eV. In all GGA calculations, the valence band maximum lies along the Σ direction. We find it worth mentioning that the indirect band gaps computed following the HF and B3LYP schemes are 10.07 and 2 eV, respectively. Thus, the band gap predicted by PBE is closer to the experimental indirect band gap ~0.84 and 1.09 eV [16,39] in comparison to other calculations. The underestimation of band gap by the DFT-GGA and overestimation by the HF schemes are well anticipated in semiconductors [40]. The gap overestimation by the HF method is usually attributed to the lack of screening. The B3LYP value of 2 eV is intermediate between GGA and HF values. This is to be expected, since this hybrid functional essentially augments the LDA and GGA by non-local exchange [40,41]. The electronic band structure for the B2 phase is plotted in Fig. 4. Figure depicts negative band gap of 0.9 eV. A similar structure is also predicted by other workers [39]. However, the band gap is quantitatively lower (~0.22 eV) than the present value.

4.4. Compton profiles

4.4.1. Directional Compton profiles

Compton profiles for B1 structure of CdO have been computed following Eq. (3) along [1 1 1], [1 1 0] and [1 0 0] directions. Due to non-availability of experimental data, these results cannot be put to any test. It is to be noted that the difference in direc-

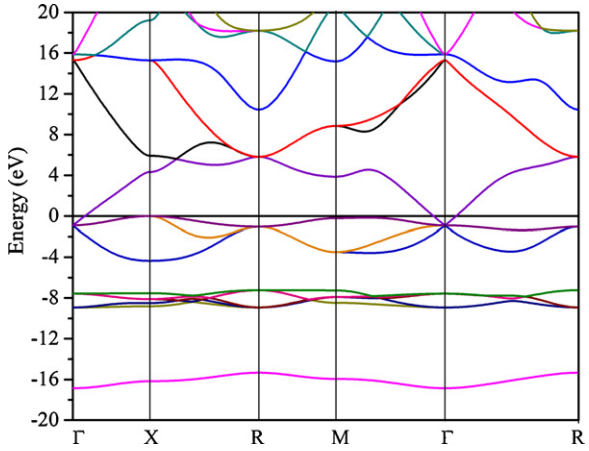

Fig. 4. Energy band structure for B2 phase of CdO obtained from the PBE correlation and Becke's exchange functional. There is a negative band gap of 0.9 eV.

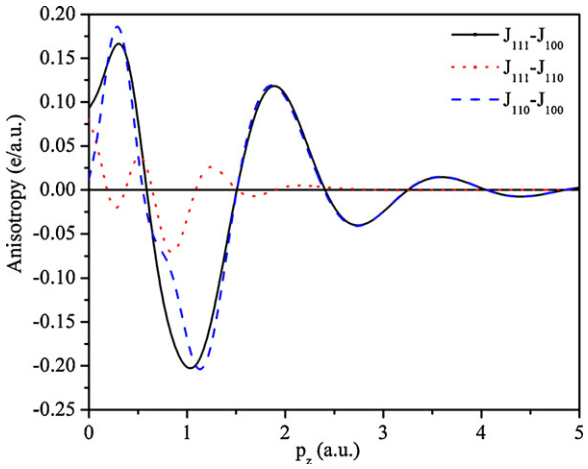

Fig. 5. Compton profile anisotropies for B1 phase CdO.

tional Compton profiles represent, in fact, anisotropy in valence electron density $\rho(\mathbf{p})$ because the difference in the isotropic contributions from inner electrons cancel out. To examine the directional features, theoretically, we plot [1 1 1]–[1 0 0], [1 1 1]–[1 1 0] and [1 1 0]–[1 0 0] anisotropies of CdO in Fig. 5. The figure depicts that all anisotropies are positive in nature around $p_z = 0$ and the maximum anisotropy is 3.4% of valence $J_{avg}(0)$. Also the anisotropy between [1 1 1] and [1 0 0] directions is maximal and shows oscillations. These oscillations are anticipated on the multiples of $2\pi/a\sqrt{3}$ (~0.4, 0.8 a.u.) and $2\pi/a\sqrt{2}$ (~0.49, 0.98 a.u.) in the anisotropies related to the [1 1 1] and [1 1 0] directions. Such oscillations are visible at 0.35 and 1 a.u. for the [1 1 1]–[1 0 0] and 0.38 and 1.15 a.u. for the [1 1 0]–[1 0 0] anisotropy. As anticipated extremes in [1 1 1]–[1 0 0] appear before [1 1 0]–[1 0 0] in Fig. 5. However, there is a subtle disagreement in the momentum where the positive and negative oscillations are predicted. Possible reasons will be discussed later when isotropic Compton profile is compared with measurement. The anisotropies with respect to [1 0 0] direction, i.e. [1 1 1]–[1 0 0] and [1 1 0]–[1 0 0] are larger in magnitude and show similar trends. The two anisotropies are visible up to 4.0 a.u. only. On the other hand, the third anisotropy, i.e. [1 1 1]–[1 1 0] is low in magnitude and exists up to 1.7 a.u. only. It clearly points that within $1.7 \le p_z \le 4.0$ a.u. range, the anisotropic behaviour in [1 1 1]–[1 0 0] and [1 1 0]–[1 0 0] is mainly from the momentum density along the [1 0 0] direction. Specifically, anisotropies in the region dominated by the valence electrons become zero at $2\pi/a \sim 0.7$, 1.4 a.u. Thus, the broad features are well reflected in anisotropies. The anisotropy in the three cases diminishes beyond 4.0 a.u. To interpret the fine features and to verify theoretical directional Compton profiles measurements on single crystalline samples are required. It is hoped that these directional Compton profiles would stimulate measurements on single crystals which would help in extracting more accurate information about the electronic structure in this material.

4.4.2. Isotropic Compton profiles

As stated earlier, we have computed Compton profiles from the DFT-LCAO method and the ionic model. In ionic model, we have considered a number of ionic arrangements $Cd^{+x}O^{-x}$ ($0.0 \le x \le 2.0$ in step of 0.1). In Table 3, we present our results on theoretical and experimental Compton profiles. In column 2, the unconvoluted spherically averaged theoretical Compton profile derived from PBE correlation functional is given. The ionic profiles for a few ionic arrangements are given in columns 3–7. The experimental Compton profile is given in the last column of the table including experimental errors at selected points. The listing of all profiles will enable usage by other workers who may perform experiment at different momentum resolution. For quantitative comparison, we convoluted all theoretical profiles with a Gaussian function of 0.6 a.u. FWHM and computed difference profiles $\Delta J = J^{Theory}(p_z) - J^{Expt.}(p_z)$. All values are normalized to 22.859 electrons within 0 to +7 a.u. range of momentum. The difference curves thus obtained from various ionic arrangements are plotted in Fig. 6. This figure depicts that the effect of charge transfer from Cd to O is largely visible within 0–2.0 a.u. range of momentum and the ionic configuration with $x = 0.1$ shows the largest deviation with the experiment around $J(0)$. The best agreement is found for $x = 0.5$. Beyond 2.0 a.u., all difference curves are identical because the contribution in this momentum region is dominated by the inner electrons, which are unaffected in the charge transfer. To check the overall agreement of all ionic configurations with the experiment

Table 3
Unconvoluted theoretical and the experimental Compton profiles of CdO. All profiles are normalized to 22.859 electrons between 0 to +7 a.u. Statistical errors ($\pm\sigma$) are given at some points. All profiles are in e/a.u.

p_z	$J(p_z)$						
	DFT-LCAO	Ionic model					Experiment
		$Cd^{+0.1}O^{-0.1}$	$Cd^{+0.3}O^{-0.3}$	$Cd^{+0.5}O^{-0.5}$	$Cd^{+0.7}O^{-0.7}$	$Cd^{+0.9}O^{-0.9}$	
0.0	10.241	11.675	11.455	11.235	11.015	10.796	10.520 ± 0.049
0.1	10.219	11.437	11.241	11.045	10.849	10.654	10.441
0.2	10.108	10.816	10.678	10.540	10.402	10.264	10.354
0.3	9.933	10.061	9.991	9.921	9.852	9.782	10.217
0.4	9.668	9.358	9.345	9.331	9.317	9.303	9.968
0.5	9.367	8.806	8.829	8.851	8.873	8.895	9.608
0.6	9.020	8.376	8.416	8.457	8.497	8.538	9.191
0.7	8.615	8.009	8.056	8.104	8.151	8.198	8.767
0.8	8.178	7.669	7.716	7.763	7.810	7.857	8.339
1.0	7.261	7.005	7.044	7.083	7.122	7.161	7.449 ± 0.041
1.2	6.420	6.321	6.351	6.381	6.411	6.442	6.564
1.4	5.695	5.651	5.674	5.697	5.720	5.744	5.734
1.6	5.017	5.007	5.025	5.043	5.061	5.079	5.032
1.8	4.410	4.423	4.437	4.451	4.465	4.479	4.438
2.0	3.886	3.906	3.917	3.928	3.939	3.950	3.913 ± 0.029
3.0	2.269	2.274	2.278	2.281	2.284	2.287	2.162 ± 0.020
4.0	1.606	1.625	1.626	1.627	1.628	1.629	1.551 ± 0.017
5.0	1.255	1.277	1.277	1.277	1.277	1.278	1.183 ± 0.014
6.0	0.996	1.017	1.017	1.018	1.018	1.018	0.951 ± 0.012
7.0	0.785	0.807	0.807	0.807	0.807	0.807	0.782 ± 0.011

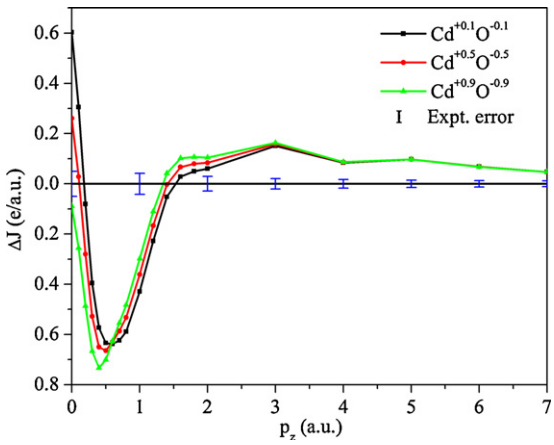

Fig. 6. Difference ($\Delta J = J^{\text{Theory}}(p_z) - J^{\text{Expt.}}(p_z)$) between convoluted ionic and experimental Compton profiles of CdO. Experimental errors ($\pm\sigma$) are also shown at some points. All ionic profiles are convoluted with the Gaussian of 0.6 a.u. FWHM.

in the whole range, i.e. 0 to +7 a.u., we have computed χ^2 given as:

$$\chi^2 = \sum_{p_z=0}^{7.0} \left| \frac{\Delta J(p_z)}{\sigma(p_z)} \right|^2, \quad (4)$$

where $\sigma(p_z)$ is the corresponding experimental error. On the basis of χ^2 test and Fig. 6, we infer that $Cd^{+0.5}O^{-0.5}$ configuration gives the best agreement suggesting transfer of 0.5 electrons from the valence 5s state of Cd to the 2p state of O. Despite such an agreement residual differences are visible in the curve which are not unexpected while noting the fact that these values are based on free atom profiles, without considering crystalline effects. To examine this, we present the difference curves of convoluted DFT-LCAO and the best agreed ionic arrangement ($Cd^{+0.5}O^{-0.5}$) with the experiment in Fig. 7. The figure reveals that differences shown by the DFT-LCAO are smaller in comparison to the ionic profile in the ($0.2 \le p_z \le 7$ a.u.) momentum range. In the ($0.0 \le p_z \le 0.2$ a.u.) range ionic profile shows better agreement than the DFT-LCAO method. The maximum difference shown by the DFT-LCAO with experiment is about 5.3% of $J(0)$ compared to 6.3% by the ionic profile. The differences of both the schemes with measurement are beyond experimental errors. To check overall agreement of the two calculations with the experiment in the whole range, i.e. 0 to +7 a.u., we computed χ^2 defined in Eq. (4). On the basis of χ^2 check and

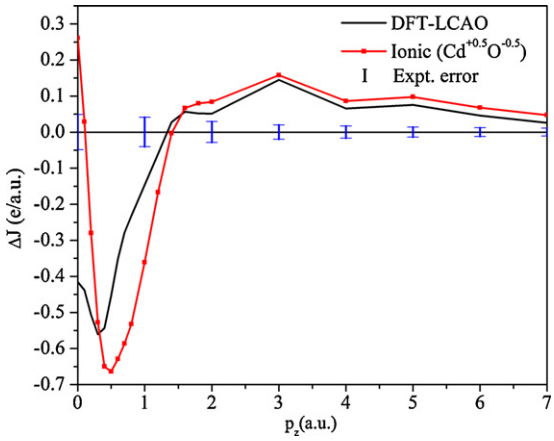

Fig. 7. Difference ($\Delta J = J^{\text{Theory}}(p_z) - J^{\text{Expt.}}(p_z)$) between convoluted theoretical Compton profiles (PBE and the best ionic) and the experimental Compton profile. Experimental errors ($\pm\sigma$) are also shown at some points. All profiles are convoluted with the Gaussian of 0.6 a.u. FWHM.

Fig. 7, we infer that DFT-LCAO shows better agreement than the ionic model. Figure also reveals that, except at $p_z = 0.0$ and 0.1 a.u., both DFT-LCAO and ionic arrangement underestimate the Compton profile in the momentum region ($0.0 \le p_z \le 1.4$ a.u.). Beyond, 1.4 a.u. the trend is reverse. The underestimation by the DFT-LCAO within ($0.0 \le p_z \le 1.4$ a.u.) suggests a lower contribution of sp valence electrons in theory as these electrons have prominent contribution in this region and as a consequence of normalisation, it causes disagreement beyond 1.4 a.u. As the p and d bands have anisotropic character, it is likely that hybridisation of these bands may produce quantitatively different contribution in the momentum density and hence Compton profiles. It may thus shift the occurrence of positive and negative oscillations on the momentum scale in Fig. 5 and account for the subtle disagreement. Although DFT-LCAO has shown an improvement in agreement with measurement, there are residual differences in the difference curves below 1.4 a.u. These residual differences may probably get reduced by having more accurate basis sets which may also help in bringing down the differences in low momentum region particularly due to sp valence states. However, such calculations would need high-resolution measurements for critical examination.

5. Conclusions

In this work structural and electronic ground state properties of CdO are determined. The structural properties namely equilibrium lattice constant, bulk modulus, pressure coefficient for the B1 and B2 structures are computed following the DFT-LCAO method. It has been found that B1 is energetically favorable state under ambient conditions. Using PBE correlation functional, the structural parameters for both phases are reasonably in good agreement with the experimental data. Our calculation shows B1 → B2 structural phase transition at 102.5 GPa in good agreement with the experiments. Electronic band structure calculations show that B1 phase of CdO is semiconductor with indirect band gap of 0.43 eV. The B2 phase of CdO has negative band gap of 0.9 eV.

X-ray structure factors for a few reflection lines of B1 and B2 structures of CdO are provided. For the B1 structure it is seen that up to (2 2 0) reflection the agreement is good and within experimental errors. Beyond this, differences are larger than the experimental errors. The present study demands more accurate measurement of X-ray structure factors for rigorous analysis. Compton profile measurement on polycrystalline CdO supports the DFT-LCAO calculation than simple ionic model. The simple ionic model suggests transfer of 0.5 electrons from 5s state of Cd to 2p state of O. Broad features in the oscillatory behaviour of anisotropies are well explained on the basis of directional characteristics. The theoretical anisotropies with respect to [1 0 0] direction, i.e. [1 1 1]–[1 0 0] and [1 1 0]–[1 0 0] are larger in magnitude and show similar trends suggesting that the two anisotropies are dominated by the momentum density along [1 0 0] direction in the $1.5 \le p_z \le 4.0$ a.u. range of momentum. More accurate basis sets especially for the sp valence states may probably be helpful to estimate all these properties more accurately. Measurements on single crystalline samples with better resolution and high statistics will be very helpful to examine these findings rigorously.

Acknowledgements

UP is grateful to the CSIR, New Delhi for awarding JRF. Financial support given by the UGC, New Delhi through Emeritus Fellowship and SR/33-37/2007 to BKS and post-doctoral fellowship to RKK is gratefully acknowledged. MSD is thankful to Prof. M.P. Poonia, Principal, Engineering College, Bikaner for providing computational facilities.

References

[1] I. Hamberg, C.G. Granqvist, J. Appl. Phys. 60 (1986) R123.
[2] T.J. Coutts, D.L. Young, X. Li, W.P. Mulligan, X. Wu, J. Vac. Sci. Technol. A 18 (2000) 2646.
[3] T. Minami, Semicond. Sci. Technol. 20 (2005) S35.
[4] Y.Z. Zhu, G.D. Chen, H. Ye, A. Walsh, C.Y. Moon, S.-H. Wei, Phys. Rev. B 77 (2008) 245209.
[5] A. Schleife, C. Rödl, F. Fuchs, J. Furthmüller, F. Bechstedt, Phys. Rev. B 80 (2009) 35112.
[6] P.D.C. King, T.D. Veal, P.H. Jefferson, J. Zúñiga-Pérez, V. Muñoz-Sanjosé, C.F. McConville, Phys. Rev. B 79 (2009) 35203.
[7] P.M. Devshette, N.G. Deshpande, G.K. Bichile, J. Alloys Compd. 463 (2008) 576.
[8] A.A. Dakhel, Thin Solid Films 518 (2010) 1712.
[9] A.A. Dakhel, J. Alloys Compd. 475 (2009) 51.
[10] A.A. Dakhel, Solar Energy 83 (2009) 934.
[11] A.A. Dakhel, Opt. Mater. 31 (2009) 691.
[12] F. Peng, D. Chen, H. Fu, X. Cheng, Phys. Status Solidi B 246 (2009) 71.
[13] Y. Duan, L. Quinn, G. Tang, L. Shi, Eur. Phys. J. B 66 (2008) 201.
[14] R.J. Guerrero-Moreno, N. Takeuchi, Phys. Rev. B 66 (2002) 205205.
[15] H. Liu, H-K. Mao, M. Somayazulu, Y. Ding, Y. Meng, D. Häusermann, Phys. Rev. B 70 (2004) 94114.
[16] Y. Dou, R.G. Egdell, D.S.L. Law, N.M. Harrison, B.G. Searle, J. Phys. Condens. Matter 10 (1998) 8447.
[17] P.D.C. King, T.D. Veal, A. Schleife, J. Zúñiga-Pérez, B. Martel, P.H. Jefferson, F. Fuchs, V. Muñoz-Sanjosé, F. Bechstedt, C.F. McConville, Phys. Rev. B 79 (2009) 205205.
[18] E. Rantavuori, V.-P. Tanninen, Phys. Scr. 15 (1977) 273.
[19] B. Williams, Compton Scattering, McGraw-Hill, London, 1977.
[20] M.J. Cooper, Rep. Prog. Phys. 48 (1985) 415.
[21] M.J. Cooper, P.E. Mijnarends, N. Shiotani, N. Sakai, A. Bansil (Eds.), X-ray Compton Scattering, Oxford Publishing Press, 2004.
[22] R. Dovesi, R. Orlando, C. Roetti, C. Pisani, V.R. Saunders, Phys. Status Solidi B 217 (2000) 63.
[23] C. Pisani, R. Dovesi, C. Roetti, Hartree-Fock Ab initio Treatment of Crystalline Solids, Lecture Notes in Chemistry, vol. 48, Springer-Verlag, Heidelberg, 1988.
[24] W. Kohn, L.J. Sham, Phys. Rev. 140 (1965) A1133.
[25] V.R. Saunders, R. Dovesi, C. Roetti, M. Causua, N.M. Harrison, R. Orlando, C.M. Zicovich-Wilson, CRYSTAL98 User's Manual, University of Torino, 1998.
[26] http://www.tcm.phy.cam.ac.uk/.
[27] J.P. Perdew, K. Burke, M. Ernzerhof, Phys. Rev. Lett. 77 (1996) 3865.
[28] J.P. Perdew, K. Burke, M. Ernzerhof, Phys. Rev. Lett. 78 (1997) 1396(E).
[29] F. Tran, R. Laskowski, P. Blaha, K. Schwarz, Phys. Rev. B 75 (2007) 115131.
[30] F. Birch, J. Geophys. Res. 83 (1978) 1257.
[31] P. Coppens, X-ray Charge Density and Chemical Bonding, Oxford University Press, 1997.
[32] F. Biggs, L.B. Mandelsohn, J.B. Mann, At. Data Nucl. Data Tables 16 (1975) 201.
[33] B.K. Sharma, A. Gupta, H. Singh, S. Perkkiö, A. Kshirsagar, D.G. Kanhare, Phys. Rev. B 37 (1988) 6821.
[34] S. Perkkiö, B.K. Sharma, S. Manninen, T. Paakkari, B.L. Ahuja, Phys. Status Solidi B 168 (1991) 657.
[35] D.N. Timms, Ph.D. thesis (unpublished), University of Warwick, England, 1989.
[36] J. Felsteiner, P. Pattison, M.J. Cooper, Phil. Mag. 30 (1974) 537.
[37] A. Mujica, A. Rubio, A. Munoz, R.J. Needs, Rev. Mod. Phys. 75 (2003) 863.
[38] S. Limpijumnong, W.R.L. Lambrecht, Phys. Rev. Lett. 86 (2001) 91.
[39] A. Schleife, F. Fuchs, J. Furthmüller, F. Bechstedt, Phys. Rev. B 73 (2006) 45212.
[40] F. Bechstedt, F. Fuchs, G. Kresse, Phys. Status Solidi B 246 (2009) 1877.
[41] M. Neef, K. Doll, G. Zwicknagl, J. Phys. Condens. Matter 18 (2006) 7437.
[42] H. Liu, J.S. Tse, H. Mao, J. Appl. Phys. 100 (2006) 93509.